AIAA JOURNAL
Vol. 49, No. 8, August 2011

Cyclic Buckling Tests Under Combined Loading on Predamaged Composite Stiffened Boxes

P. Cordisco* and C. Bisagni†
Politecnico di Milano, 20156 Milano, Italy

DOI: 10.2514/1.J050999

The results obtained on two predamaged closed boxes composed of four graphite-epoxy curved stiffened panels are presented. One panel of each box is predamaged, using Teflon inserts between three stringers and the skin to reproduce skin-stringer disbonding. The boxes are tested under axial compression and torque, applied individually and in combination, both statically and cyclically. The tests allow the investigation of the effect of static and cyclic postbuckling combined loads in terms of structural behaviors, of collapse modalities and of damage propagation. The boxes do not suffer any loss of structural performances or any predamage propagation for combined loading under small compression and torsion up to 275% of the buckling torque, which corresponds to 85% of the collapse torque.

I. Introduction

RECENT advances in the graphite-epoxy materials have increased the number of aerospace industries that use these materials in primary aerospace structures. These advances did not yet bring a total comprehension of their behavior and, consequently, too conservative safe margins are still used. For example, nowadays, the designers place the buckling load close to the limit load [1], even if it is well known that graphite-epoxy structures can deeply work in the postbuckling field [2–5].

One of the reasons can be found in the fact that even if some efforts have been done for understanding the damage mechanisms induced by a postbuckling load [6–9], the studies are mainly numerical or consider composite specimens under static conditions. Few data are available in literature dealing with full-scale buckling tests of composite aerospace structures [10–12], and even less on structures subjected to cyclic postbuckling loads [13–15]. Consequently, the effect of a repeated postbuckling load on the global behavior and on the damage propagation is not yet fully understood. In any case, further weight savings could be obtained if the capability of such structures is demonstrated to operate in the postbuckling field thousands of times without losing efficiency, to include the buckling load in the range of the loads allowed during the operative life. Moved by this consideration, during the last years some research projects have been funded to deeply investigate, both numerically and experimentally, the behavior of graphite-epoxy aerospace primary structures in the postbuckling field [1].

The work presented here describes part of the results obtained by Politecnico di Milano during the European research project COCOMAT [1] (Improved Material Exploitation at Safe Design of Composite Airframe Structures by Accurate Simulation of Collapse), which aims to exploit the structural behavior between the buckling load and the collapse load of graphite-epoxy stiffened panels by means of experimental static and cyclic tests, and to develop validated tools able to capture the damage mechanisms leading to collapse.

During the project, Politecnico di Milano tested five structural boxes, each one composed of four CFRP curved stringer stiffened panels. Two boxes were nominally undamaged, and the remaining three boxes presented some predamaged areas, obtained using Teflon inserts between three stringers and the skin, in order to simulate skin-stringer disbonding. Results achieved on the undamaged boxes were already published by the same authors [15], and this paper presents the results obtained on two predamaged boxes, tested under axial compression and torsion, applied individually and in combination. One of the boxes is tested by static loading, and both static and cyclic tests are performed on the second box, to investigate the effects of repeated postbuckling combined loads on the structural behavior and on the predamage propagation.

II. Structures

The work presented here is part of a larger experimental campaign carried out at the Politecnico di Milano within the COCOMAT project. During the project, five boxes were tested under combined axial compression and torque.

At the beginning, two boxes were investigated. The first one (box SN1) was tested under static loads, and the second one (box SN2) was tested under static and cyclic loads. Then, three boxes were analyzed considering predamaged areas, obtained with Teflon inserts between three stringers and the skin. The first structure (box SN3) was tested under static loads, and the other two (box SN4 and box SN5) were tested under static and cyclic loads. In particular, box SN4 was tested in the same conditions and number of cycles of box SN2, and box SN5 with higher loads and a higher number of cycles. All the five boxes were then collapsed in the same static condition with compression and torsion. In this way, it was possible to find out, on one hand, the influence that static and cyclic combined postbuckling loads have on undamaged and predamaged structures and, from the other hand, the effect that initial predamages have on the global response of these structures in the postbuckling field up to collapse. The results obtained in the tests carried out on the undamaged boxes have already been presented by the same authors in a previous paper [15], and the results achieved on two of the three predamaged structures (box SN3 and box SN5) are presented here.

The structures (Fig. 1) were manufactured by AgustaWestland in unidirectional and fabric graphite-epoxy material.

Each box is composed of four panels. Two of them are large panels, 700 mm wide, with four stringers, and the other two are small panels, 242 mm wide, with one stringer in the middle. All the panels present a radius of curvature of 1500 mm and a height of 700 mm. The stringers are made with both unidirectional and fabric plies, and

Presented at the AIAA/ASME/ASCE/AHS/ASC Structures, Structural Dynamics, and Materials Conference, Palm Springs, CA, 4–7 May 2009; received 13 October 2010; revision received 17 January 2011; accepted for publication 19 January 2011.

*Postdoctoral Fellow, Department of Aerospace Engineering, Via La Masa 34.

†Associate Professor, Department of Aerospace Engineering, Via La Masa 34. Senior Member AIAA.

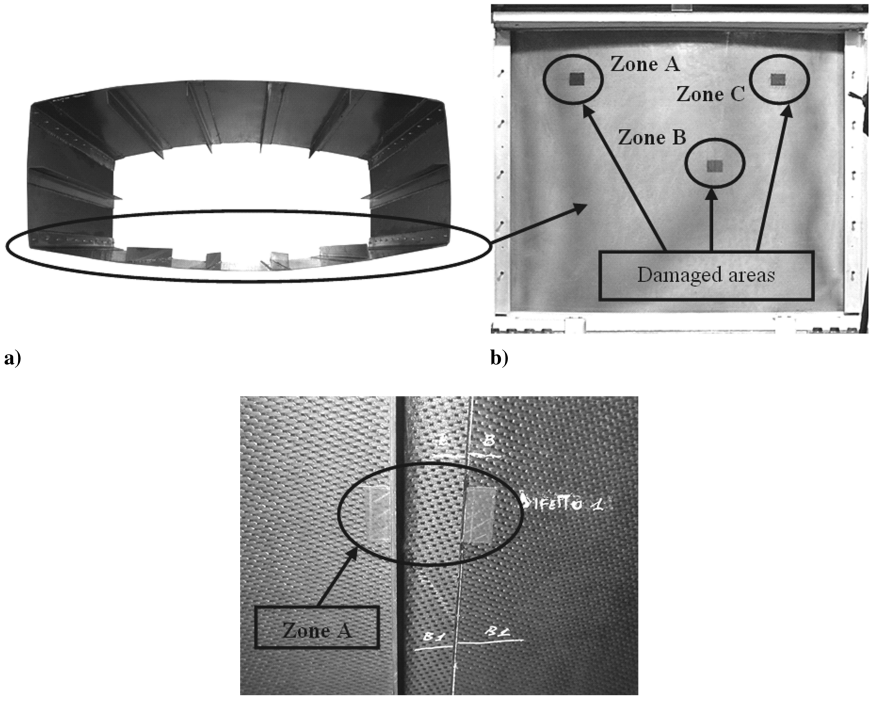

Fig. 1 Closed box: a) top view, b) predamage location, and c) inner view of one Teflon insert.

the skin with only fabric plies. The layup and the thickness of the skin and of the stringers are reported in Table 1. The stringers are L-shaped with a section of 28 × 28 mm and a height of 700 mm, and are bonded to the panel skin after the curing process. Large and small panels are joined together with four more stringers as connection elements. The connection stringers are identical to the other stringers, but present an angle between the flanges equal to 107° instead of 90°, and are applied at the corners of the box using both glue and rivets.

Teflon inserts are placed between three stringers and the skin of the front panel of the boxes, to obtain three predamaged areas representative of skin-stringer disbonding. The areas are 28 mm high and spread for the entire stringer width. The damage locations are determined by the industrial partners, according to their experience in manufacturing and operations.

The boxes are bonded into two aluminum ending tabs to allow the clamping on the loading machine. A dedicated equipment is used to assure that the ending tabs are plane and parallel, in order to guarantee the uniform distribution of the load during the tests. The free length of the box results consequently reduced to 640 mm.

Each box is instrumented with 72 strain gauges, whose position is reported in Fig. 2. In particular, the strain gauges are placed in back-to-back configuration on one of the large panels (back panel) and on the two small lateral panels. On the remaining large panel (front panel), the strain gauges are bonded only internally, to leave the external surface free for the measurements of the out-of-plane displacements with the laser sensor and for the ultrasound inspections.

III. Experimental Equipment

The buckling tests are performed with the loading equipment described in previous papers by the same authors [15,16]. The equipment, shown in Fig. 3, allows axial compression and torsion to be applied, both individually and in any required combination. The axial compression can be applied only statically, and it is possible to apply torsion both statically and cyclically. Both compression and torsion are controlled in displacement.

Table 1 Thickness and layup of skin and stringers

Parameter	Value[a]
Skin thickness	0.99 mm
Skin layup	$[0°_F/-45°_F/0°_F]$
Stringer thickness	2.22 mm
Stringer layup	$[0°_F/0°_{UD}/0°_{UD}/+45°_F/0°_{UD}/0°_{UD}/-45°_F/0°_{UD}/0°_{UD}/0°_F]$

[a]F is fabric and UD is unidirectional.

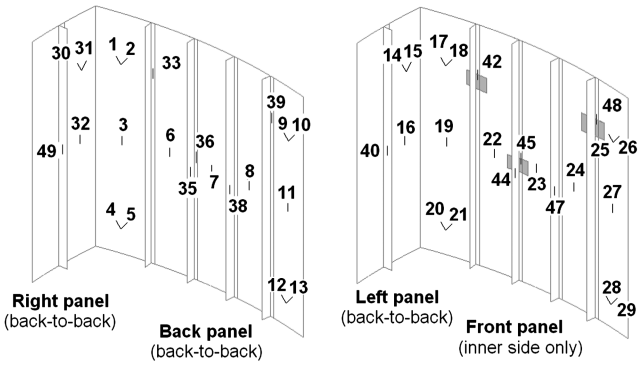

Fig. 2 Strain-gauge map (predamaged areas in light gray).

During the buckling tests, the evolution of the out-of-plane displacements of the box front panel is measured using ad hoc developed laser equipment, placed in front of the buckling test equipment. It is based on a laser sensor that has the ability to translate horizontally and vertically with respect to the testing structure. Ad hoc developed software processes the acquired data and generates the 3-D plots of the scanned surface.

A moiré fringes frame is realized in order to visualize the out-of-plane displacements of the box during the tests. Moreover, an ultrasound (US) system has been set up to allow the damage investigations through C-scan using a 22 MHz US probe directly in situ during the tests.

IV. Testing Methodology

The testing procedure for the two nominally identical boxes is decided together with AgustaWestland. The first box (box SN3) is tested under static loading, and the second box (box SN5) is tested under static and cyclic loading.

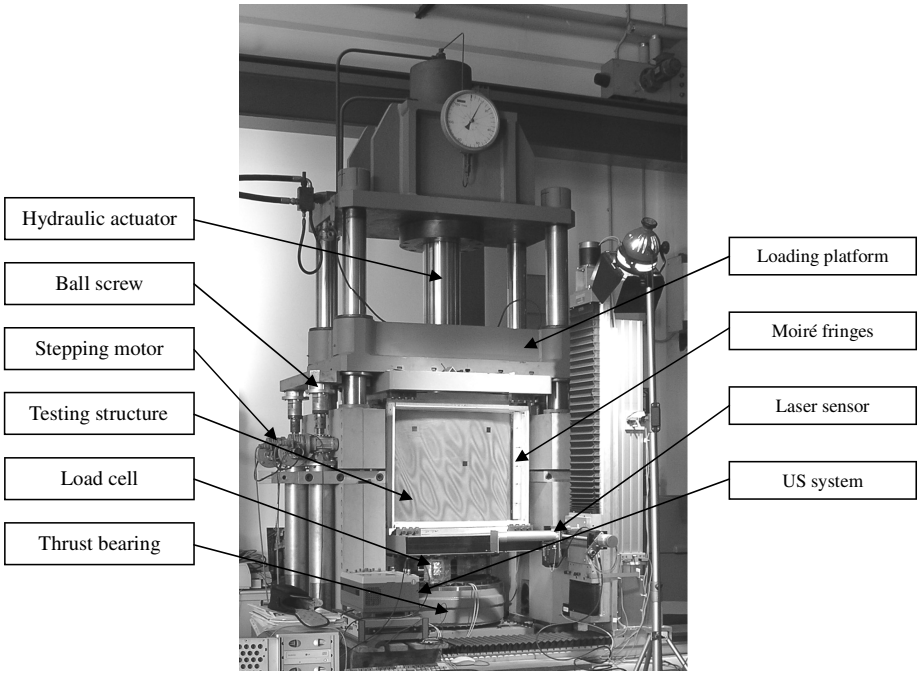

Fig. 3 Buckling test equipment.

On box SN3, 28 static buckling tests are performed. At the beginning, a pure axial compression test, a pure clockwise (CW) torque test and a pure counterclockwise (CCW) torque test are carried out. Then, eight interaction tests are performed using three different procedures. In the first procedure, the axial compression is fixed to constant values, equal to 25, 50, 75, and 95% of the buckling load measured in the pure axial compression test, and the postbuckling field is reached increasing the torque, both in clockwise and in counterclockwise direction. In the second procedure, the torque is fixed to constant values, equal to the buckling torque recorded in the eight tests performed with the first procedure, and the postbuckling field is reached increasing the axial compression. In the third procedure, the axial compression and the torque are increased by steps equal to 5% of the buckling loads measured in the tests carried out with the first procedure. In all the combined tests, the maximum reached value is 125% of the buckling load. Box SN3 is then tested until collapse keeping the axial compression load equal to 50% of the buckling load measured in the pure axial compression

Table 2 Overview of experimental tests

Test type	Load conditions
	SN3 box, static tests
Pure compression	Compression
Pure torque	CCW torque and CW torque
Combined (24 tests)	Constant compression plus CW or CCW torque
	Constant CW or CCW torque plus compression
	Compression plus CW or CCW torque increased by steps
Collapse	Constant compression plus CCW torque
	SN5 box, static tests
Pure compression	Compression
Pure torque	CCW torque
Combined (4 tests)	Constant compression plus CCW torque
	SN5 box, cyclic tests
Cyclic	Constant compression plus $0 <$ CCW torque $< 125\% T_{\mathrm{BUCK}}$
Cyclic	Constant compression plus $0 <$ CCW torque $< 150\% T_{\mathrm{BUCK}}$
Cyclic	Constant compression plus $0 <$ CCW torque $< 175\% T_{\mathrm{BUCK}}$
Cyclic	Constant compression plus $0 <$ CCW torque $< 200\% T_{\mathrm{BUCK}}$
Cyclic	Constant compression plus $0 <$ CCW torque $< 225\% T_{\mathrm{BUCK}}$
Cyclic	Constant compression plus $0 <$ CCW torque $< 250\% T_{\mathrm{BUCK}}$
Cyclic	Constant compression plus $0 <$ CCW torque $< 275\% T_{\mathrm{BUCK}}$
Cyclic	Constant compression plus $0 <$ CCW torque $< 300\% T_{\mathrm{BUCK}}$
Collapse	Constant compression plus CCW torque

Table 3 Results of axial compression and torque tests on box SN3 and box SN5

Test	Measure	SN3	SN5	Difference %
Axial compression	Buckling load	74.1 kN	67.4 kN	−9.0
Axial compression	Initial stiffness	225.3 kN/mm	220.6 kN/mm	−2.1
Torque	Buckling torque	7.2 kNm	7.0 kNm	−2.9
Torque	Initial stiffness	27.2 kNm/ deg	26.1 kNm/ deg	−4.2

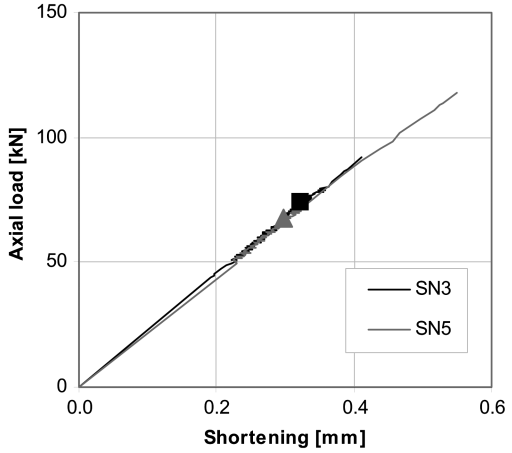

Fig. 4 Axial-load-vs-shortening relationships measured during compression tests on box SN3 and box SN5.

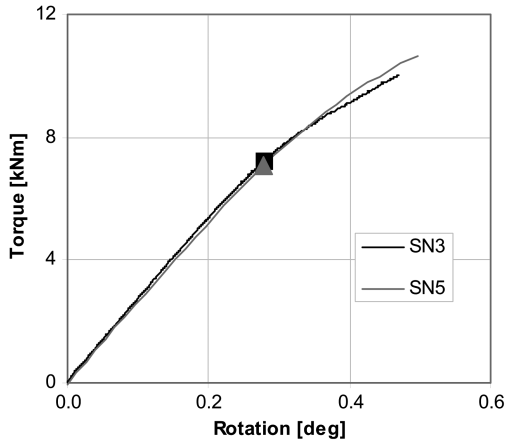

Fig. 5 Torque-vs-rotation relationships measured during torsion tests on box SN3 and box SN5.

test, and reaching the collapse by increasing the torque in the counterclockwise direction.

On box SN5, six initial static tests are at first performed in order to measure the counterclockwise part of the interaction relationship: a pure axial compression test, a pure counterclockwise torque test, and four combined tests in the counterclockwise direction according to the first procedure. Box SN5 is then tested under cyclic loading, keeping the axial compression load equal to 50% of the buckling load obtained in the pure axial compression test and cycling in torsion. Calling T_{BUCKL} the buckling torque of the box, eight cyclic sequences are performed at 0.2 Hz: 1) 2000 cycles from 0 to 125% T_{BUCKL}, 2) 2000 cycles from 0 to 150% T_{BUCKL}, 3) 2000 cycles from 0 to 175% T_{BUCKL}, 4) 2000 cycles from 0 to 200% T_{BUCKL}, 5) 2000 cycles from 0 to 225% T_{BUCKL}, 6) 10000 cycles from 0 to 250% T_{BUCKL}, 7) 2000 cycles from 0 to 275% T_{BUCKL}, and 8) 1000 cycles from 0 to 300% T_{BUCKL}.

For the cyclic sequence at 250% T_{BUCKL}, it is decided to perform 10000 cycles in order to also investigate the effect of the number of cycles before reaching load levels close to collapse. The sequence at 300% T_{BUCKL} is stopped after about 1000 cycles because of visible damage on the box.

Every 2000 cycles, the torque-vs-rotation relationship, the strain-gauge measurements, the laser scan of the box front panel and the US inspection of the predamaged areas are recorded. Box SN5 is then statically tested until collapse, performing the collapse test in the same condition of the collapse test of box SN3.

All of the tests performed on the two boxes and the load sequences are summarized in Table 2.

V. Experimental Results

The results of the experimental tests are presented in four different sections, in order to evaluate the structural behavior and the predamages evolution considering the following aspects: 1) buckling behavior, 2) effect of loading sequence, 3) effect of cyclic postbuckling loading, and 4) collapse modalities.

A. Buckling Behavior

The two boxes are initially tested under pure axial compression and under pure torque to record the static behavior. The tests are performed until 125% of the buckling loads, except for the test under axial compression on box SN5, where a load equal to 175% of the buckling one is reached on box SN5 in order to verify that no buckling of the stringers is obtained until this load.

The buckling loads are identified using back-to-back strain gauges. It must be taken into account that it is difficult to exactly determine the first buckling load, due to the difficulty of unambiguously defining the buckling onset and due to the limited number of strain gauges.

The prebuckling stiffness of the boxes is calculated as the slope up to 85% of the buckling load. Results obtained in the pure axial compression and in the pure torque tests on both boxes are compared in Table 3, where box SN3 is taken as reference.

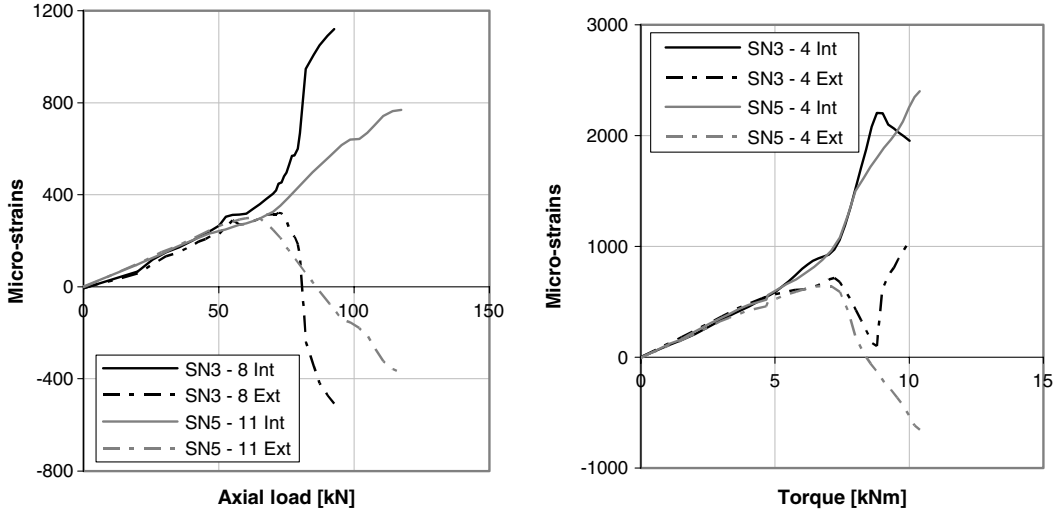

a) b)

Fig. 6 Measurements of back-to-back strain gauges of boxes SN3 and SN5: a) Axial compression test and b) torsion test.

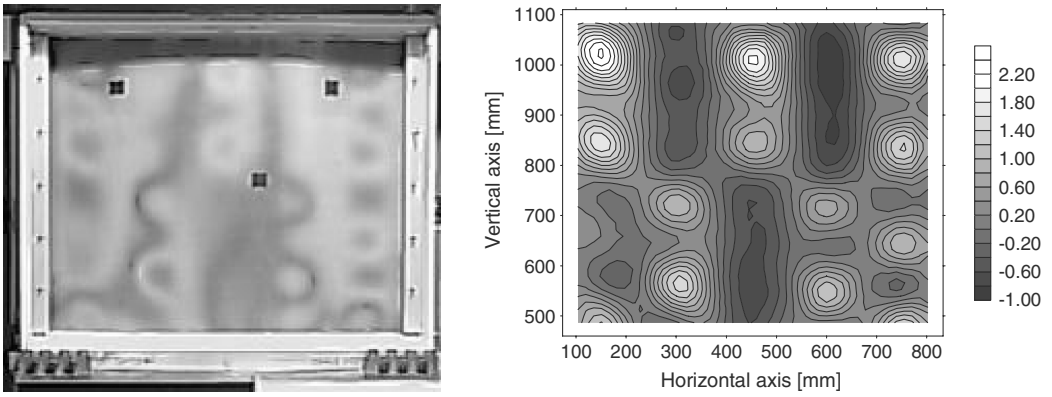

a) Axial compression load = 119.6 kN

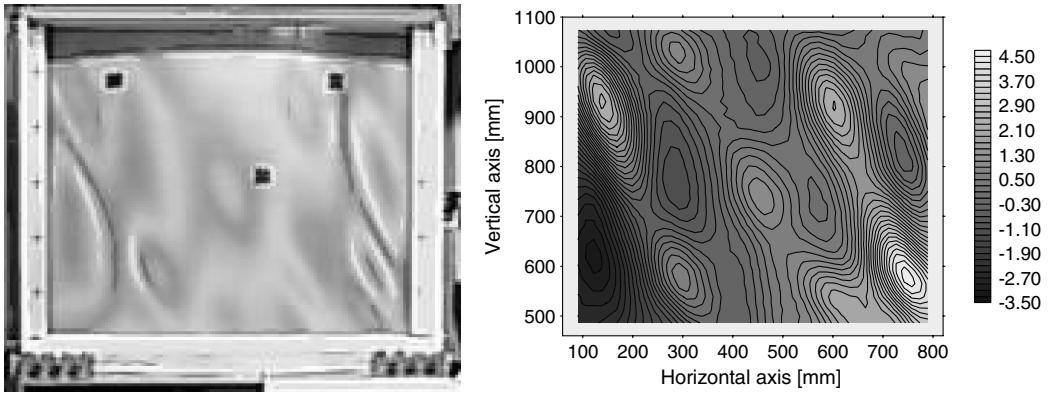

b) CCW Torque = 10.6 kNm

Fig. 7 Photographs with moiré fringes and laser measurements of box SN5: a) axial compression test and b) torsion test.

The comparison between the relationships of axial compression vs shortening and the relationships of torque vs rotation is shown in Figs. 4 and 5, respectively, where the buckling loads are highlighted.

Even if the boxes are nominally identical, some differences are measured, especially in the buckling loads: box SN5 shows lower buckling loads, both under axial compression (9.0%) and torque (2.9%). Moreover, box SN5 is globally slightly less stiff, both under axial compression (2.1%) and under torque (4.2%).

Comparing the measurements of some back-to-back strain gauges (Fig. 6), it is possible to observe that the initial strain distribution is the same for the two boxes, but then the strain gauges bonded on box SN5 measure lower buckling loads.

The postbuckling deformation of the two boxes is very similar in the buckles distribution and in the maximum out-of-plane displacements, both under axial compression and under torque. Photographs with the moiré fringes and the laser contour plots taken at maximum load in the tests carried out on box SN5 are shown in Fig. 7. The out-of-plane displacements reach 2.4 mm inward and 0.9 mm outward in the axial compression test, and 4.5 mm inward and 3.5 mm outward in the torsion test.

B. Effect of Loading Sequence

The effect of the application sequence of static combined postbuckling loading on the buckling behavior is investigated considering the tests carried out on the first box, and the effect of static combined postbuckling loading on the predamages propagation is analyzed from the tests carried out on both boxes.

Twenty-seven static tests are performed on box SN3 before the collapse: a pure axial compression test, two pure torque tests, one in the clockwise and one in the counterclockwise direction, and 24 combined axial compression and torque tests, which are carried out

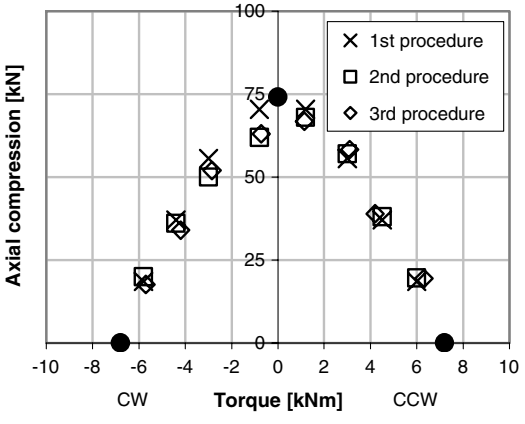

Fig. 8 Interaction relationships of box SN3.

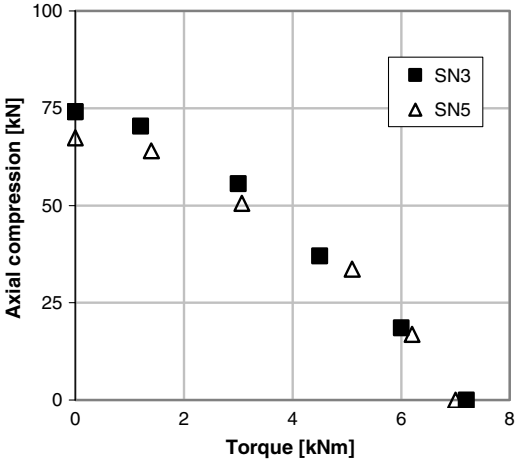

Fig. 9 Comparison of CCW interaction relationships of box SN3 and box SN5.

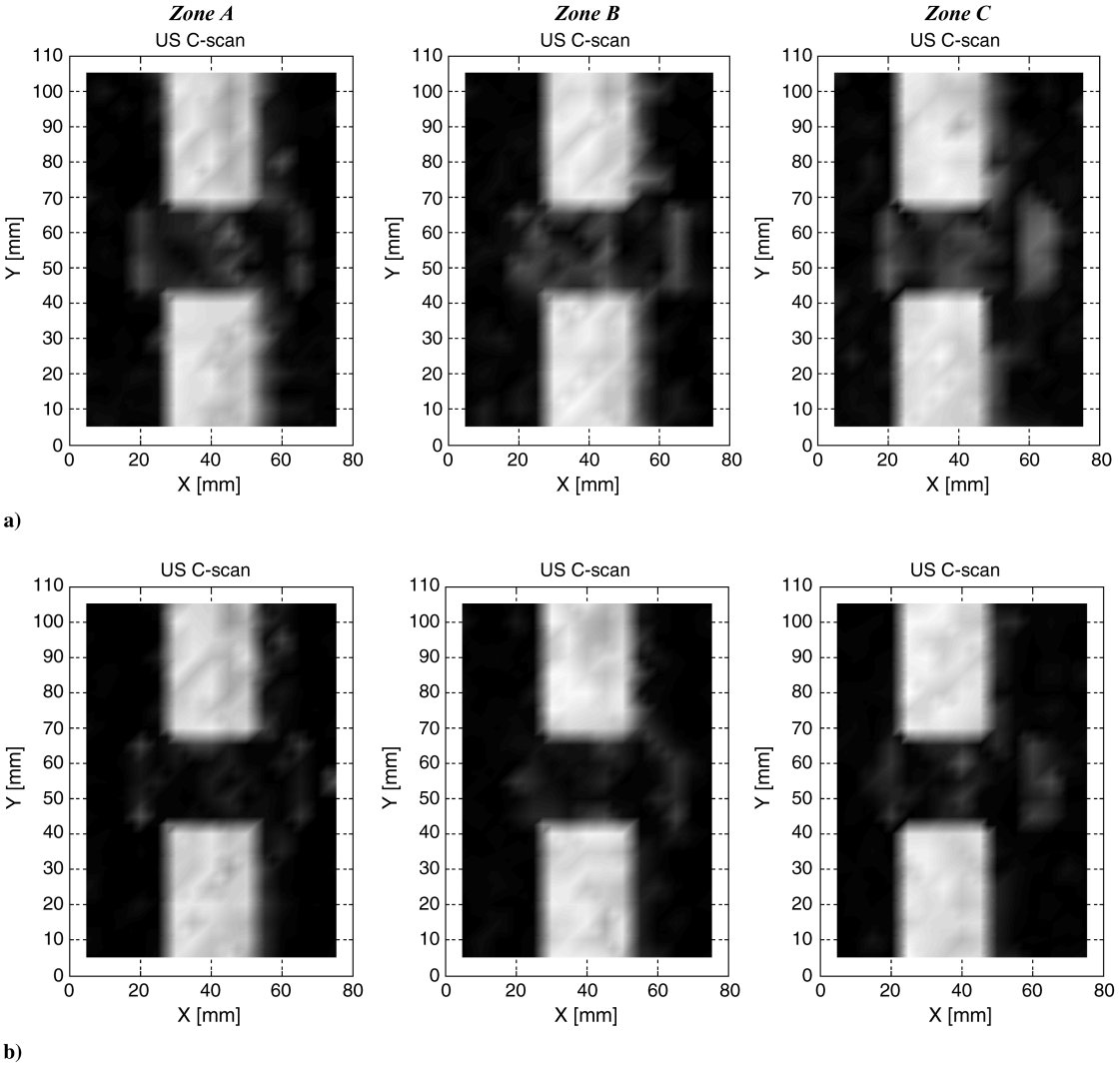

Fig. 10 US inspections on box SN5: a) C-scans before tests and b) C-scans after static tests.

with three different procedures. The interaction relationships measured using the three different loading procedures are presented in Fig. 8. The buckling torques achieved in the pure clockwise and in the pure counterclockwise torque tests are different due to nonsymmetric L-shaped section of the stringers and bend–twist anisotropy in the skin. Observing the buckling values and the interaction relationships, it appears that different loading sequences do not significantly affect the buckling under combined loads. It means, for example, that applying an axial compression followed by a torque or a torque followed by an axial compression causes the box to buckle practically at the same load. There is only one set of data points associated with −1 kNm that shows a 10–12% difference between the first load procedure and the second and third procedures. In this case, the compression is predominant, so the effect of imperfection is more significant. During the first procedure, only for one load combination, a small barely visible buckle appeared in a different location from the other ones. The buckling load was also identified by the strain gauges for the point of the first load procedure, even if a buckle was already a little visible in another area. It is important to note that it is difficult to exactly determine the first buckling load, due to the difficulty of unambiguously defining the buckling onset and due to the limited number of strain gauges.

On box SN5 six static tests under combined postbuckling loads are performed with the first procedure, allowing to measure the counterclockwise part of the interaction relationship. Box SN3 and box SN5 present a very close behavior, as shown in Fig. 9, where the counterclockwise part of the interaction relationships are sketched.

The US inspections of the three predamaged areas are taken, for both boxes, before and after all the static tests, to evaluate if the combined postbuckling loads can imply a damage propagation. The comparison of the obtained C-scans shows that no damage propagation is achieved. As an example, the C-scans obtained for box SN5 are presented in Fig. 10.

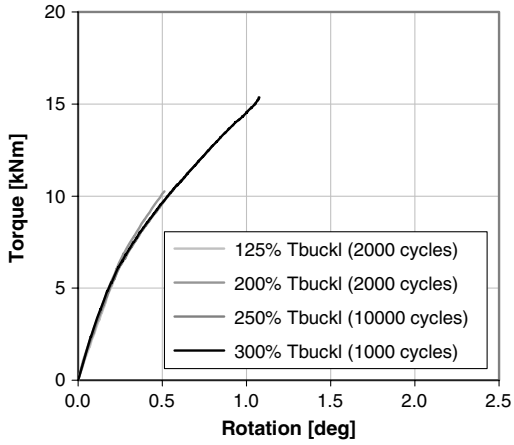

Fig. 11 Torque-vs-rotation relationships measured during cyclic sequences on box SN5.

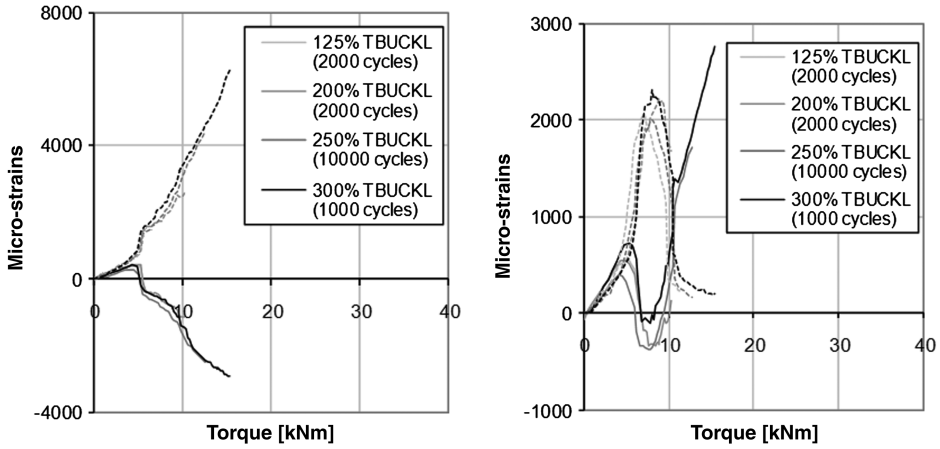

a) b)

Fig. 12 Comparison of strain-gauge relationships measured during cyclic sequences on box SN5; strain gauges of a) the skin of the back panel and b) the skin of the back panel (solid line: internal strain gauge; dotted line: external strain gauge).

C. Effect of Cyclic Postbuckling Loading

The effect of cyclic postbuckling combined loading on the global response of the structures and on the damage propagation can be obtained from the results of box SN5.

Indeed, after the six preliminary static tests, box SN5 is subjected to eight cyclic postbuckling loading sequences under combined axial compression and torque. Every 2000 cycles, the behavior of the box is investigated by recording the torque-vs-rotation relationship, by acquiring the strain gauges, by measuring the deformed shape with the laser system and by scanning the predamaged areas with the US system.

The comparison of the torque-vs-rotation relationships taken at the beginning of some cyclic sequences is shown in Fig. 11. It can be observed that there is no remarkable change in the global behavior of the box due to the cyclic postbuckling loading.

The same observation can be done comparing the strain-gauge measurements. As an example, the relationships measured by two couples of back-to-back strain gauges are presented in Fig. 12.

Even the deformed shape of the box front panel scanned by the laser equipment is not affected by the cycles, as it can be concluded observing Fig. 13, where the C-scans taken before and after the sequence at 175% T_{BUCKL} and before and after the sequence at 250% T_{BUCKL} are presented.

The last cyclic sequence, performed fixing the axial compression to 33.7 kN and cycling the torque from 0 to 15.3 kNm (i.e., 300% T_{BUCKL}) is stopped after about 1000 cycles because of the separation

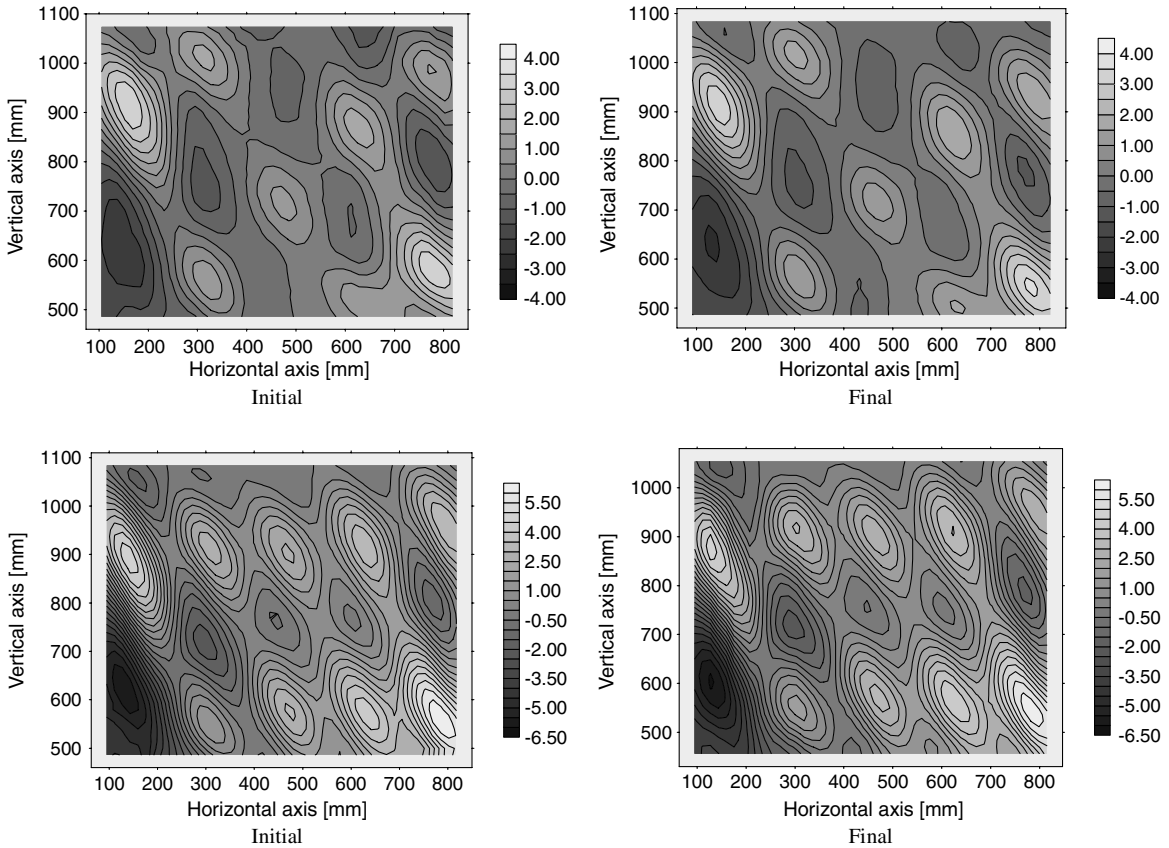

Fig. 13 Comparison of laser measurements during two cyclic sequences on box SN5: a) 2000 cycles at 175% T_{BUCKL} and b) 10,000 cycles at 250% T_{BUCKL}.

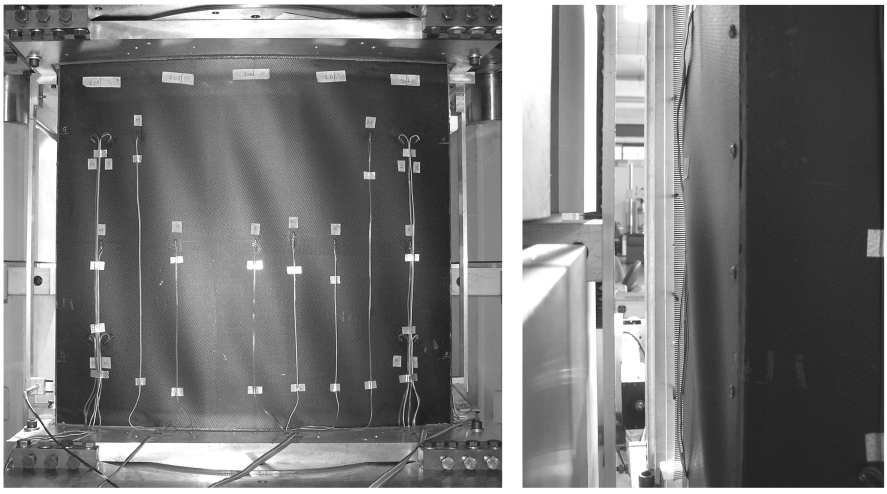

a) b)

Fig. 14 Box SN5 after the cyclic sequence at 300% T_{BUCKL}: a) back panel and b) front panel.

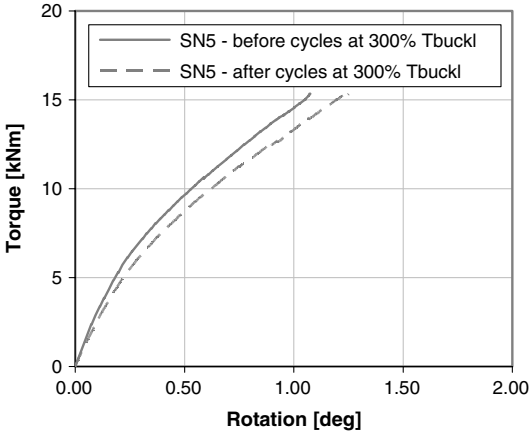

Fig. 15 Torque-vs-rotation relationships of box SN5 obtained during the cyclic sequence at 300% T_{BUCKL}.

between the stringer and the skin of one of the box lateral panels. The back panel and the lateral panel are shown in Fig. 14. A buckle that considers the full panel width is visible in Fig. 14b. The buckle goes from the back panel to the front panel, and it is no longer limited by the central stringer of the lateral panel. Because of this separation, the structural stiffness of the box decreases, as shown in Fig. 15, where the torque-vs-rotation relationships measured at the beginning and at the end of the cyclic sequence at 300% T_{BUCKL} are reported. It can be pointed out that this is a very high load, and that up to 275% of the buckling load the structure has sustained the cyclic loading without any damages.

Moreover, no propagation of the predamages on the front panel is obtained, as it is clear comparing the US scans of the predamaged areas taken at the beginning of all the tests (Fig. 10) and those taken at the end of the last cyclic sequence (Fig. 16).

D. Collapse Modalities

The two boxes are then tested until collapse in the same conditions, increasing the torque in the counterclockwise direction while keeping the axial compression equal to 50% of the buckling load measured in the pure axial compression test. The results obtained in the collapse tests performed on the first box, tested only under static loads, are compared with those obtained on the second box, tested under static and cyclic loads.

The data obtained in the collapse tests on the two boxes are summarized in Table 4, where box SN3 is taken as reference. The comparison of the torque-vs-rotation relationships is presented in Fig. 17. It is possible to note that the difference in the first buckling torque is equal to 13.3%. Moreover, large differences are recorded in the stiffness: the prebuckling stiffness (calculated as the slope up to 85% T_{BUCKL}) of box SN5 is 11.3% lower than the one of box SN3, and the difference in the postbuckling stiffness

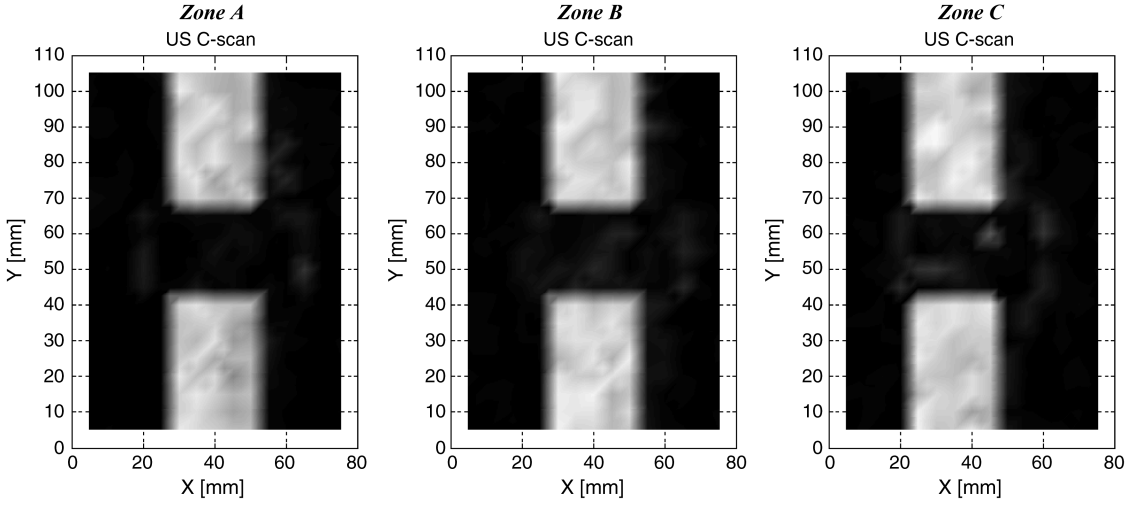

Fig. 16 US inspections on box SN5 after cyclic sequences.

Table 4 Results of collapse tests on box SN3 and box SN5

	SN3	SN5	Difference %
Constant axial compression	37.0 kN	33.7 kN	−8.9
Buckling torque	4.5 kNm	5.1 kNm	13.3
Collapse torque	18.0 kNm	18.2 kNm	1.1
Initial stiffness	27.6 kNm/ deg	24.3 kNm/ deg	−11.3
Postbuckling stiffness	10.4 kNm/ deg	8.5 kNm/ deg	−18.3
Ratio between collapse load and buckling load	4.0	3.6	−10.0

(calculated as the slope from 200% T_{BUCKL} to 300% T_{BUCKL}) is equal to 18.3%.

These differences are caused by the separation between the stringer and the skin of the lateral panel of the box SN5 achieved during the cyclic sequence at 300% T_{BUCKL}. Indeed, comparing the torque-vs-rotation relationships of box SN3 during the collapse test (plotted until 300% T_{BUCKL}) with the relationship obtained for box SN5 at the beginning of the cyclic sequence at 300% T_{BUCKL} (Fig. 18), it is possible to conclude that the behavior of the two boxes would have been similar until that load, before the separation of the stringer.

The evolution of the out-of-plane displacements of the two boxes are reported for similar torque values in Fig. 19 and in Fig. 20, respectively. It can be observed that they are not exactly the same, but the response is of the same type.

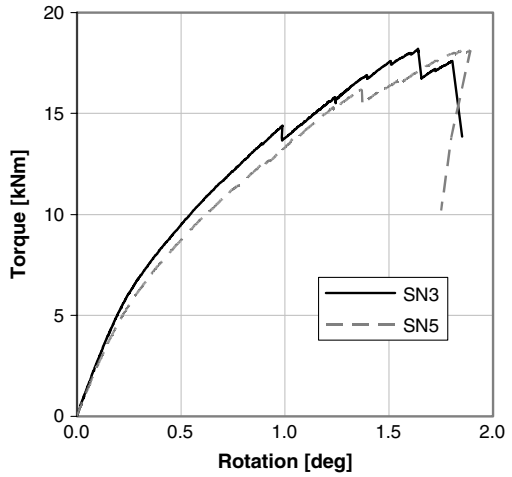

Fig. 17 Torque-vs-rotation relationships obtained in collapse tests on box SN3 and box SN5.

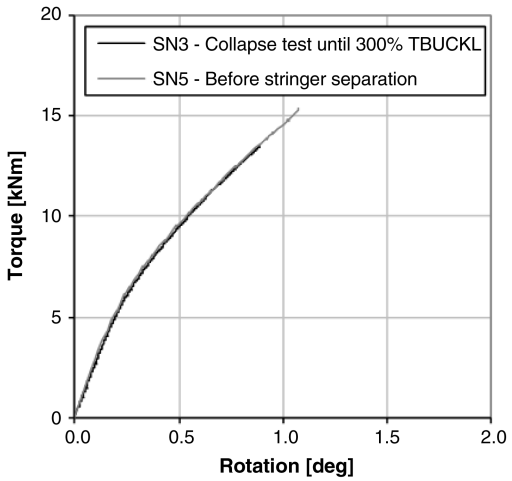

Fig. 18 Comparison between torque-vs-rotation relationships of collapse test on box SN3 and of test on box SN5 up to 300% T_{BUCKL} before the last cyclic sequence.

As far as the evolution of the deformed shape of box SN3 is concerned, the buckling torque is equal to 4.5 kNm and is characterized by a small wave on the front panel. The waves then develop in diagonal and at 7.8 kNm (Fig. 19a) the out-of-plane displacements of the contour plots are equal to 3.4 mm inward and 3 mm outward. At 10.1 kNm (Fig. 19b), the laser equipment measures waves 4.6 mm inward and 4.3 mm outward. The first failure on the box, recorded at 14.4 kNm, consists of the separation between the skin and the stiffener of the right panel, which causes a decrease of the load to 13.8 kNm. The box is still able to sustain an increase of load, so the test is continued. When the torque reaches 14.6 kNm, two rows of waves are regularly distributed all over the panels (Fig. 19c). At this load, the out-of-plane displacements are 6.8 mm deep inward and 7.2 mm deep outward. Further increasing in the torque does not change the shape any more, but only causes the waves to be deeper and deeper. At 16.9 kNm (Fig. 19d), the waves reach a maximum depth of 8 mm inward and 7.9 mm outward. At 18 kNm a second failure is achieved and the load is reduced to 16.7 kNm. This time, no visible damages or changes in the deformed shape are observed, so the test continues, until the final collapse is reached at 17.6 kNm, because of the separation between the front panel and the right one (Fig. 21). Therefore, the maximum load reached during the collapse test is 18 kNm, obtaining a ratio between the collapse load and the buckling load equal to 4.

As far as the evolution of the deformed shape of box SN5 is concerned, it buckles at 5.1 kNm, and, even in this case, the buckling is characterized by a small wave on the front panel. Increasing the torque, more waves appear along the diagonal (Fig. 20a), and at 7.6 kNm the out-of-plane displacements of the contour plots are 2.7 mm inward and 3.7 mm outward. At 10.2 kNm (Fig. 20b), the laser equipment measures deeper waves than those measured on the previous box: 5.2 mm inward and 5.6 mm outward. Moreover, even increasing the torque, no regular distribution of the buckles is observed. At 12.4 kNm, a separation between the central stringer and the skin of the box left panel is achieved, but the deformed shape of the front panel remains unchanged. At 14 kNm (Fig. 20c) the out-of-plane displacements are 7.7 mm deep inward and 8.9 mm deep outward. At 16.2 kNm, a small noise is heard and the torque drops down to 15.5 kNm. No visible damages are observed on the box, so the test continues. At 16.6 kNm (Fig. 20d) the out-of-plane displacements reach a depth of 9.1 mm inward and 9.9 mm outward. At 18.2 kNm, the box collapses because of a large rip between the left panel and the back one. The torque is reduced to 13.8 kNm and, after few minutes, also a separation between the right panel and the front one is observed, causing a further reduction in the torque to 10.2 kNm. In Fig. 22, a photograph of the box after collapse is presented. The ratio between the collapse torque and the buckling torque is equal to 3.56.

It can be observed that, even if the behavior of the two boxes during the collapse tests is not identical, the difference in the collapse torques is very low and equal to just 1.1%.

US inspections are taken several times during the collapse tests, in order to monitor the predamaged areas. For both boxes, no propagation is observed. As an example, the C-scans of the predamaged areas of box SN5 after the collapse are reported in Fig. 23. Comparing it with the C-scans taken at the beginning of all the tests (Fig. 10), it can be noted that the US inspections give practically the same initial predamaged areas.

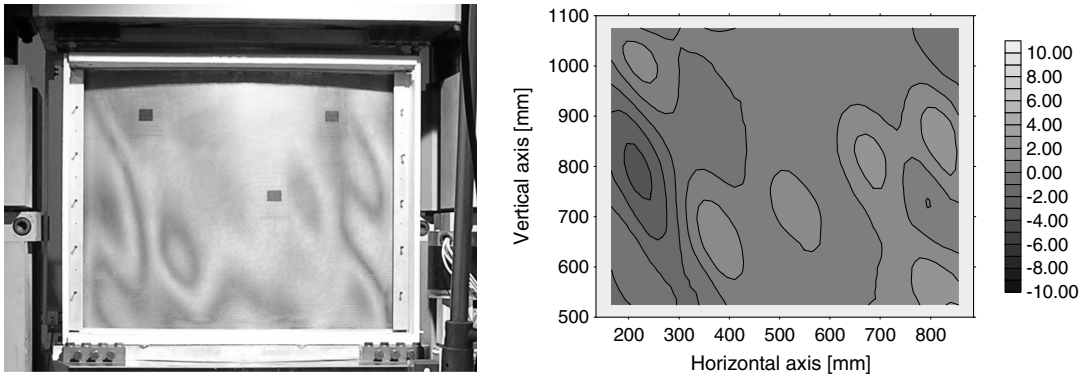

a) Torque = 7.8 kNm Axial compression = 37 kN

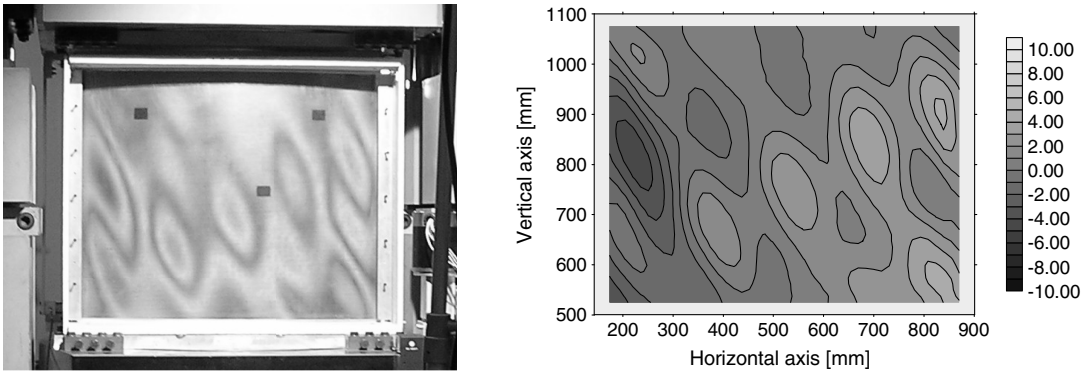

b) Torque = 10.1 kNm Axial compression = 37 kN

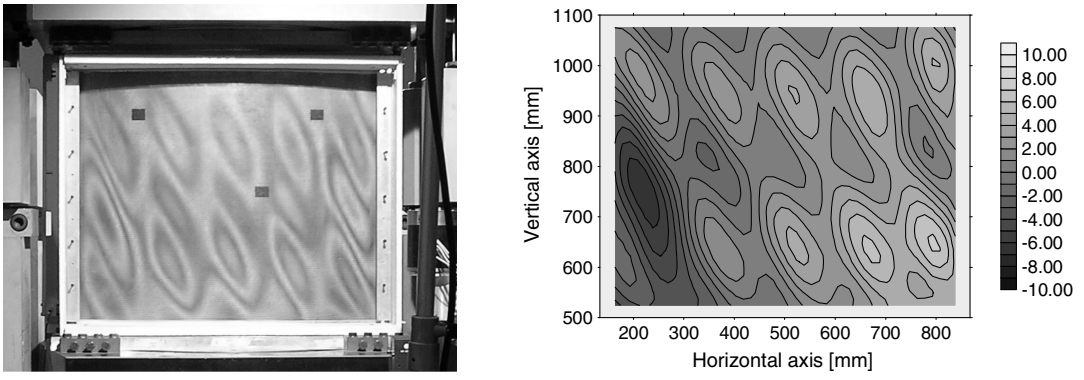

c) Torque = 14.6 kNm Axial compression = 37 kN

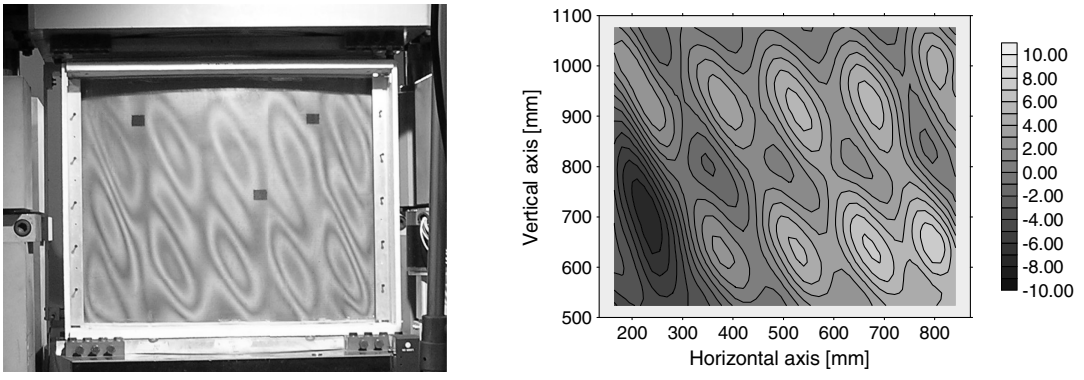

d) Torque = 16.9 kNm Axial compression = 37 kN

Fig. 19 Photographs with moiré fringes and laser measurements of box SN3 during collapse test.

The damage locations are not critical for the tested loading conditions in which the cyclic tests are dominated by shear. This type of damage and the chosen location would probably have been more critical in cyclic loading with pure compression. In any case, the chosen loading condition are typical of aircraft structures, and the predamages were chosen both for dimension and for location as one of the most critical according to the industrial partners of the COCOMAT project.

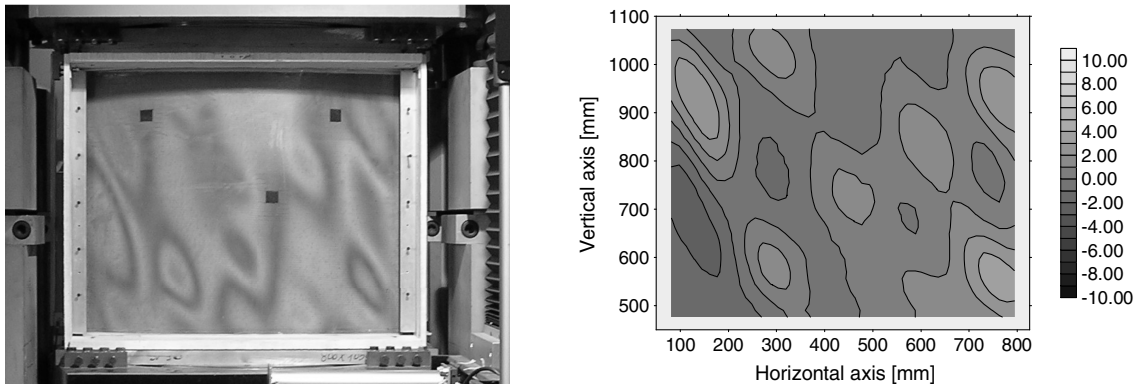

a) Torque = 7.6 kNm Axial compression = 33.7 kN

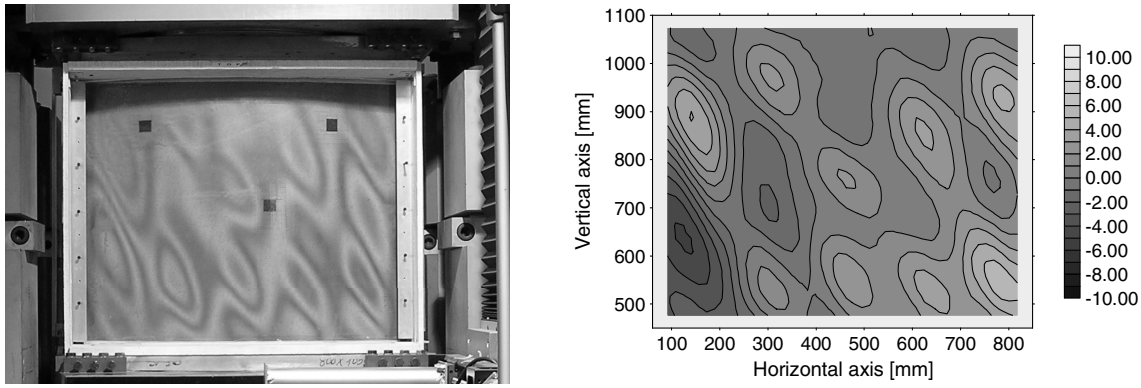

b) Torque = 10.2 kNm Axial compression = 33.7 kN

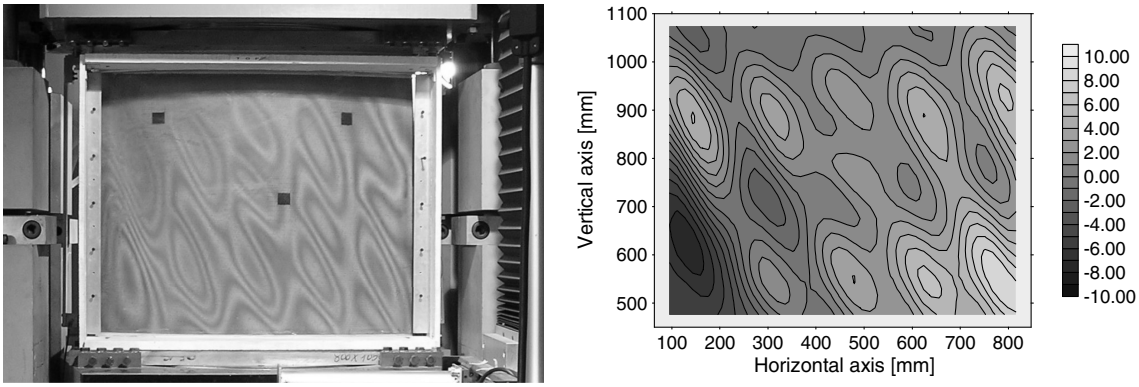

c) Torque = 14 kNm Axial compression = 33.7 kN

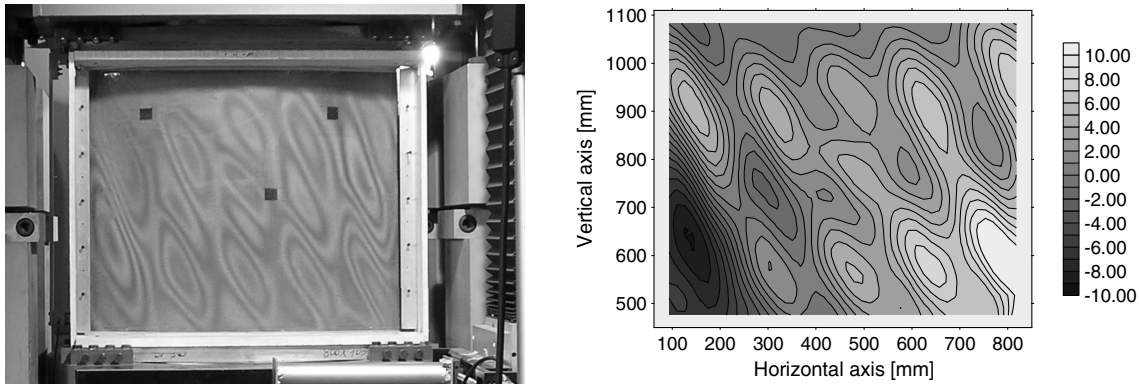

d) Torque = 16.6 kNm Axial compression = 33.7 kN

Fig. 20 Photographs with moiré fringes and laser measurements of box SN5 during collapse test.

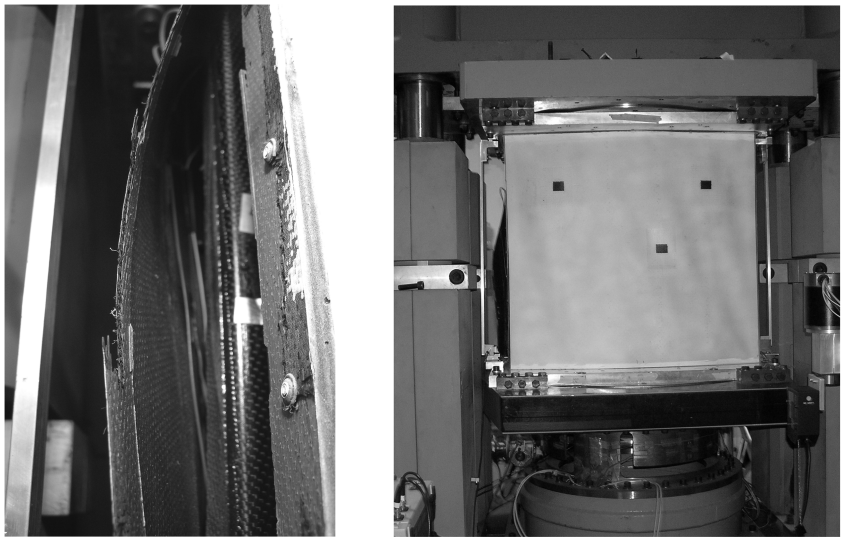

a) b)

Fig. 21 Collapse of box SN3: a) right panel and b) front panel.

a) b) c)

Fig. 22 Collapse of box SN5: a) right panel, b) front panel, and c) left panel.

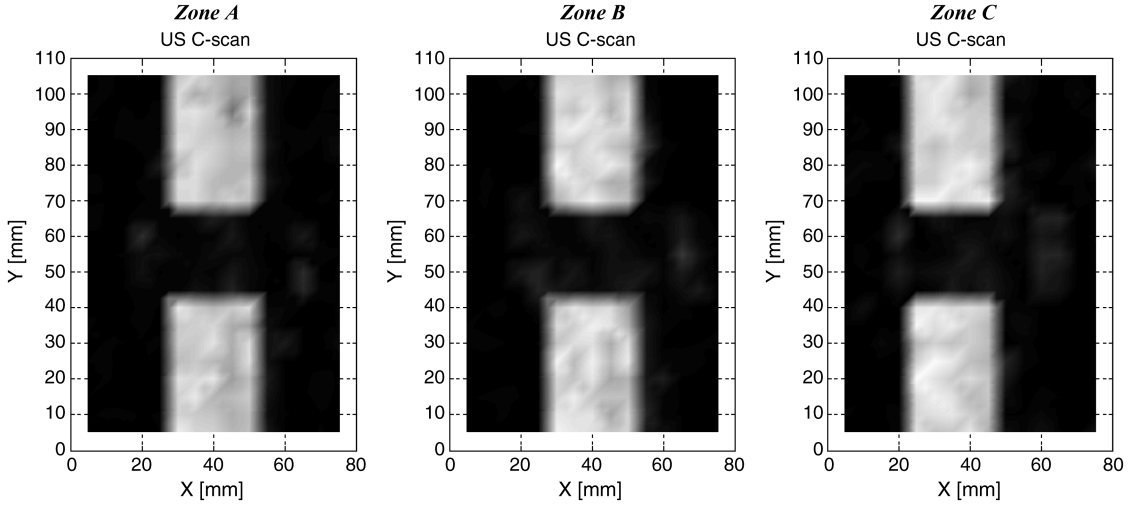

Fig. 23 US inspections on box SN5 after collapse.

VI. Conclusions

The behavior of two closed boxes composed of four graphite-epoxy curved stiffened panels has been investigated under axial compression and torque, both statically and cyclically. The front panel of each box presents three predamaged areas obtained with Teflon inserts between three stringers and the skin.

The results have been presented and compared in terms of buckling load, buckling stiffness, torque-vs-rotation relationship, deformed shape, and strain-gauge measurements. Moreover, C-scans of the predamaged areas have been carried out several times during the tests in order to monitor the evolution of the initial damages.

The performed tests allow the following observations to be reached.

First, by comparing the buckling behavior under static loading of the two boxes, it can be concluded that, even if the structures are nominally identical, some differences are obtained, probably due to the manufacturing process, but these differences are limited to 10% and mainly affect the behavior under axial compression.

Second, by comparing the effect of the loading sequence on the buckling behavior it is possible to conclude that the order of application of combined loads does not significantly change the buckling behavior. It is difficult to exactly determine the first buckling load, due to the difficulty of unambiguously defining the buckling onset and due to the limited number of strain gauges.

Third, by comparing the response of the same structure before and after the application of the cyclic postbuckling combined loading, it can be observed that the loading repetition up to 275% of the buckling torque does not influence the structural behavior, either in terms of stiffness and buckling load or in terms of deformed shapes and strain levels. Indeed, a skin-stringer separation achieved is achieved only during the cyclic sequence at 300% of the buckling torque, which corresponds to 85% of the collapse torque. This separation reduces both the prebuckling and the postbuckling stiffness of the structure. The separation has not involved the predamaged areas, as demonstrated by the US inspections and does not change the collapse torque, as the difference between the two boxes is within 2%.

It is therefore possible to conclude that the graphite-epoxy boxes investigated here show, on one hand, a large capability to safely work in the postbuckling field, reaching ratios between collapse load and buckling load higher than 3.5. On the other hand, the boxes do not suffer any loss of structural performances when they are subject to loads up to 275% of the buckling one, even if the postbuckling field is reached thousands of times. The boxes do not show any propagation of the considered predamages, either due to static or to cyclic postbuckling combined loading. Tests are planned in the near future to investigate the effect of this type of predamage in cyclic loading with pure compression, which can be more critical.

Acknowledgments

This work was supported by the European Commission, Competitive and Sustainable Growth Programme, contract no. AST3-CT-2003-502723, project COCOMAT (Improved material Exploitation at Safe Design of Composite Airframe Structures by Accurate Simulation of collapse). The information in this paper is provided as is and no guarantee or warranty is given that the information is fit for any particular purpose. The user thereof uses the information at its sole risk and liability. The authors are grateful to Vittorio Giavotto for sharing his expertise and to Daniele Mezzanzanica for his help in the ultrasound inspections.

References

[1] Degenhardt, R., Rolfes, R., Zimmermann, R., and Rohwer, K., "COCOMAT—Improved Material Exploitation at Safe Design of Composite Airframe Structures by Accurate Simulation of Collapse," *Composite Structures*, Vol. 73, No. 2, 2006, pp. 175–178. doi:10.1016/j.compstruct.2005.11.042

[2] Zimmermann, R., and Rolfes, R., "CFRP Fuselage Structures—Postbuckling Permitted," *Air & Space Europe*, Vol. 3, Nos. 3–4, 2001, pp. 129–131. doi:10.1016/S1290-0958(01)90075-9

[3] Knight, N. F., Jr., and Starnes, J. H., Jr., "Postbuckling Behavior of Selected Curved Stiffened Graphite-Epoxy Panels Loaded in Axial Compression," *AIAA Journal*, Vol. 26, No. 3, 1988, pp. 344–352. doi:10.2514/3.9895

[4] Stiftinger, M. A., Skrna-Jakl, I. C., and Rammerstorfer, F. G., "Buckling and Post-Buckling Investigations of Imperfect Curved Stringer-Stiffened Composite Shells. Part B: Computational Investigations," *Thin-Walled Structures*, Vol. 23, Nos. 1–4, 1995, pp. 339–350. doi:10.1016/0263-8231(95)00021-5

[5] Abramovich, H., Weller, T., and Bisagni, C., "Buckling Behavior of Composite Laminated Stiffened Panels Under Combined Shear-Axial Compression," *Journal of Aircraft*, Vol. 45, No. 2, 2008, pp. 402–413. doi:10.2514/1.27635

[6] Khedmati, M. R., Edalat, P., and Javidruzi, M., "Sensitivity Analysis of the Elastic Buckling of Cracked Plate Elements Under Axial Compression," *Thin-Walled Structures*, Vol. 47, No. 5, 2009, pp. 522–536. doi:10.1016/j.tws.2008.10.018

[7] Zhang, Y., and Wang, S., "Buckling, Post-Buckling and Delamination Propagation in Debonded Composite Laminates. Part 2: Numerical Applications," *Composite Structures*, Vol. 88, No. 1, 2009, pp. 131–146. doi:10.1016/j.compstruct.2008.02.012

[8] Orifici, A. C., Ortiz de Zarate Alberdi, I., Thomson, R. S., and Bayandor, J., "Compression and Post-Buckling Damage Growth and Collapse Analysis of Flat Composite Stiffened Panels," *Composites Science and Technology*, Vol. 68, Nos. 15–16, 2008, pp. 3150–3160. doi:10.1016/j.compscitech.2008.07.017

[9] Ambur, D. R., Jaunky, N., and Hilburger, M. W., "Progressive Failure Studies of Stiffened Panels subjected to Shear Loading," *Composite Structures*, Vol. 65, No. 2, 2004, pp. 129–142. doi:10.1016/S0263-8223(03)00153-3

[10] Bisagni, C., and Giavotto, V., "Experiments and Analyses on Post-Buckling Behavior of Stringer-Stiffened Laminated Composite Helicopter Tailplanes," *Journal of the American Helicopter Society*, Vol. 54, No. 2, 2009, Paper 022003. doi:10.4050/JAHS.54.022003

[11] Greenhalgh, E., Meeks, C., Clarke, A., and Thatcher, J., "The Performance of Post-Buckled CFRP Stringer-Stiffened Panels Containing Defects and Damage," 44th AIAA/ASME/ASCE/AHS Structures, Structural Dynamics, and Materials Conference, AIAA Paper 2003-1680, Norfolk, VA, 2003.

[12] Faggiani, A., and Falzon, B., "Optimization Strategy for Minimizing Damage in Postbuckling Stiffened Panels," *AIAA Journal*, Vol. 45, No. 10, 2007, pp. 2520–2528. doi:10.2514/1.26910

[13] Weller, T., and Singer, J., "Durability of Stiffened Composite Panels Under Repeated Buckling," *International Journal of Solids and Structures*, Vol. 26, No. 9, 1990, pp. 1037–1069. doi:10.1016/0020-7683(90)90016-O

[14] Abramovich, H., Singer, J., and Weller, T., "Repeated Buckling and Its Influence on the Geometrical Imperfections of Stiffened Cylindrical Shells Under Combined Loading," *International Journal of Non-Linear Mechanics*, Vol. 37, No. 4–5, 2002, pp. 577–588. doi:10.1016/S0020-7462(01)00085-3

[15] Cordisco, P., and Bisagni, C., "Cyclic Buckling Tests of Stiffened Composite Curved Panels Under Compression and Shear," *AIAA Journal*, Vol. 47, No. 12, 2009, pp. 2879–2893. doi:10.2514/1.42309

[16] Bisagni, C., and Cordisco, P., "Testing of Stiffened Composite Cylindrical Shells in the Postbuckling Range Until Failure," *AIAA Journal*, Vol. 42, No. 9, 2004, pp. 1806–1817. doi:10.2514/1.6088

M. Hyer
Associate Editor